Annals of Nuclear Energy 140 (2020) 107118

Contents lists available at ScienceDirect

Annals of Nuclear Energy

journal homepage: www.elsevier.com/locate/anucene

Numerical investigation on the effects of geometric deviations and materials properties on flow-induced deflections of fuel plates ☆

Javier González Mantecón [a,*], Miguel Mattar Neto [b]

[a] Department of Engineering Physics, McMaster University, 1280 Main Street West, Hamilton, Ontario L8S 4L8, Canada
[b] Instituto de Pesquisas Energéticas e Nucleares, IPEN-CNEN/SP, Av. Prof. Lineu Prestes 2242 – Cidade Universitária, CEP 05508-000 São Paulo, SP, Brazil

ARTICLE INFO

Article history:
Received 23 April 2019
Received in revised form 7 October 2019
Accepted 9 October 2019
Available online 25 October 2019

Keywords:
Parallel-plate fuel element
Multiphysics analysis
Critical fluid velocity

ABSTRACT

This work describes multiphysics analyses conducted to investigate the effect of geometric deviations and materials properties on flow-induced deflections of fuel plates. The analyzed configuration consists of two fuel plates and each one of them is bounded by two fluid channels. The fluid-dynamic forces acting on the plates are calculated using a Computational Fluid Dynamics model and the structural response is determined by means of a Finite Element Analysis model. Both models are coupled using the two-way fluid-structure interaction approach. The results show that manufacturing deviations from the nominal conditions and the increment of the system temperature lead to reduce the critical fluid velocity of the assembly.

1. Introduction

In parallel-plate fuel elements (see Fig. 1), a phenomenon called *hydroelastic instability* of the fuel plates has been identified. Its nature is that the motion of the plates alters the fluid-dynamic forces acting over them. As a result, these plates extract energy from the fluid flow in such a way that excessive deflections, eventually permanent deformation, or collapse may occur. This behavior may produce local overheating of the plates and perhaps a complete blockage of the flow channels. The fluid velocity at which that event occurs is named the *critical velocity* of the fuel assembly. Thus, the estimation of this velocity is essential to establish operating conditions and safety limitations of the reactors.

Daniel Miller was the first to propose a formula for predicting the critical flow velocity of fuel elements (Miller, 1958). He estimated it based on the interaction between the changes in cross-sectional areas, coolant velocities and pressures in two adjacent flow channels. For a multiple plate assembly with the long edges fixed, "Miller's velocity" is defined as:

$$v_M = \left[\frac{15Ea^3h}{\rho w^4(1-\upsilon^2)}\right]^{1/2} \quad (1)$$

In the equation E is the Young's Modulus of elasticity, ρ is the density of the coolant, υ the Poisson's ratio, $a$the fuel plate thickness, h the flow channel thickness and w the wetted width of the fuel plate or flow channel width.

The main drawback of Miller's model is that the 3D effects of the system are neglected. He considered the plate to be a wide beam and assumed a central portion of the plate. Hence, Eq. (1) neglects any local effects happening near the upstream or downstream edges. To date, Miller's theory is applied during the design of new fuel elements. Reference (IAEA, 1980) recommends that the coolant velocity through the fuel assemblies should be limited to two-thirds of the critical value given by Miller.

In the last decade, the interest in the performance of parallel-plate fuel elements has increased because a new monolithic low enriched uranium (LEU) configuration is under evaluation to replace current high enriched uranium (HEU) fuel plates (Lemoine and Wachs, 2007), which lead to somewhat thinner plates and increased fluid velocities. Consequently, the plates may be more susceptible to flow-induced deflections. In Brazil, with the construction of a new research reactor, there has also been growing attention on the fluid-structure interaction (FSI) phenomenon occurring in parallel plate assemblies. Additionally, few works have been done to comprehend the effects of deviations from the nominal geometric parameters and materials properties on the hydroelastic instability of the fuel plates.

The study presented herein, by conducting multiphysics simulations using Finite Element Analysis (FEA) and Computational Fluid Dynamics (CFD) codes, was undertaken to investigate the

☆ The analyses here presented were conducted by Javier González Mantecón during his doctoral studies at IPEN-CNEN/SP.

* Corresponding author.
E-mail address: gonzaj10@mcmaster.ca (J. González Mantecón).

https://doi.org/10.1016/j.anucene.2019.107118
0306-4549/

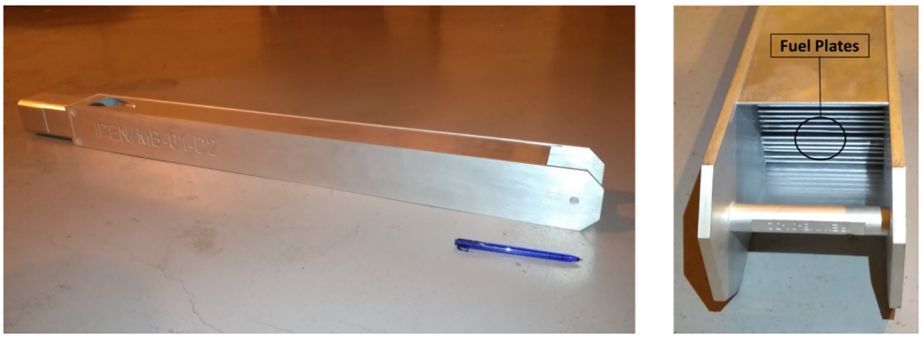

Fig. 1. Example of a fuel element used in research reactors.

influence of manufacturing deviations and the change of materials properties due to the increment of temperature on the critical velocity and deflection of fuel plates. For these purposes, nonlinear multiphysics models were developed. These models include fluid and solid fields. The domain is composed of two parallel plates and each of them is bounded by two coolant channels. The two-way fluid-structure interaction technique was utilized to couple both fields.

Based on the geometric and hydraulic characteristics of a typical fuel element of the future Brazilian Multipurpose Reactor (RMB, acronym in Portuguese) (Perrotta and Soares, 2015), this work consists of three different cases:

- Case A: Considers an array of two equal plates and three-equal flow channels, all with thicknesses smaller than the nominal dimensions, and materials properties at room temperature (24 °C).
- Case B: Considers the same plates of Case A, coolant channels with different thicknesses and materials properties at room temperature.
- Case C: Considers the plates and coolant channels with nominal dimensions and materials properties at operating temperatures, i.e. an average temperature of 50 °C and 120 °C for the fluid flow and the plates were set, respectively. The latter is approximately the maximum temperature that can be reached in a fuel plate during normal operation.

Cases A and B were motivated by Kane (1963), who described the effect of the size of inlet spacing deviations on the plate deflection. As a result of the fabrication process, some channels and/or fuel plates could have smaller dimensions. That's why, in these two cases, we considered that the thicknesses of the coolant channels and fuel plates deviated from the nominal dimensions of the assembly given in Case C. The last case was inspired by Miller (1958) who mentioned that thermoelastic instability is another source of instability. According to Miller, "it may arise due to the effects of fuel-plate deflection upon flow distribution and heat transfer".

2. Numerical approach

Our investigation was conducted using a partitioned method. On the fluid side, ANSYS CFX was utilized, and the structural side was solved with ANSYS Mechanical. For the two-way FSI simulations, the ANSYS MFX coupling algorithm was employed.

2.1. Governing equations of the fluid domain

In the present study, a three-dimensional, transient, incompressible, and turbulent flow is considered. By considering a single-phase Newtonian fluid, the Reynolds-Averaged Navier-Stokes (RANS) equations were chosen to model this fluid flow. These equations are given below:

$$\frac{\partial \rho}{\partial t} + \frac{\partial}{\partial x_j}(\rho \overline{U_j}) = 0 \tag{2}$$

$$\frac{\partial}{\partial t}(\rho \overline{U_i}) + \frac{\partial}{\partial x_j}(\rho \overline{U_i U_j}) = -\frac{\partial \overline{p}}{\partial x_i} + \frac{\partial}{\partial x_j}\left[\mu\left(\frac{\partial \overline{U_i}}{\partial x_j} + \frac{\partial \overline{U_j}}{\partial x_i}\right) - \rho\overline{u_i' u_j'}\right] + S_M \tag{3}$$

In these equations $i,j = 1,2,3$; $\overline{U}$ is the time-averaged velocity component, ρ the fluid density, μ the dynamic viscosity and S_M is the momentum source. The Reynolds stress $\rho\overline{u_i' u_j'}$ must be modeled to close the system of equations. Its value is calculated with turbulence models, such as the k-ε model.

In the standard k- ε model, two additional transport equations are solved:

$$\frac{\partial}{\partial t}(\rho k) + \frac{\partial}{\partial x_j}(\rho U_j k) = \frac{\partial}{\partial x_j}\left[\left(\mu + \frac{\mu_t}{\sigma_k}\right)\frac{\partial k}{\partial x_j}\right] + P_k + P_{kb} - \rho\varepsilon \tag{4}$$

$$\frac{\partial}{\partial t}(\rho \varepsilon) + \frac{\partial}{\partial x_j}(\rho U_j \varepsilon) = \frac{\partial}{\partial x_j}\left[\left(\mu + \frac{\mu_t}{\sigma_\varepsilon}\right)\frac{\partial \varepsilon}{\partial x_j}\right] + \frac{\varepsilon}{k}(C_{\varepsilon 1}P_k + C_{\varepsilon 1}P_{\varepsilon b} - C_{\varepsilon 2}\rho\varepsilon) \tag{5}$$

where k is the turbulence kinetic energy, μ_t the turbulence viscosity, and ε is the turbulence eddy dissipation. These equations contain five constants: $C_\mu = 0.09$, $C_{\varepsilon 1} = 1.44$, $C_{\varepsilon 2} = 1.92$, $\sigma_k = 1.0$ and $\sigma_\varepsilon = 1.3$. These constants have been obtained by means of comprehensive data fitting for a wide variety of turbulent flows (Launder and Spalding, 1974). P_k represents the turbulence production due to viscous forces, P_{kb} and $P_{\varepsilon b}$ are the influence of the buoyancy forces, correspondingly (ANSYS Inc., 2017a).

2.2. Governing equations of the solid domain

The calculations for the structural part are based on impulse conservation. It is solved using a finite element approach. The dynamic response of the structure herein analyzed is described as follows:

$$[M]\ddot{\boldsymbol{x}} + [C]\dot{\boldsymbol{x}} + [K]\boldsymbol{x} = \boldsymbol{F}(t) \tag{6}$$

in which $[M]$ is the mass matrix of the structure, $\ddot{\boldsymbol{x}}$ the nodal acceleration vector, $[C]$ the damping matrix, $\dot{\boldsymbol{x}}$the nodal velocity vector, $[K]$ the stiffness matrix, $\boldsymbol{x}$the nodal displacement vector, and $\boldsymbol{F}(t)$ the total load vector changing with time.

2.3. Interface conditions

In fluid-structure problems, the mechanical quantities of the two fields are exchanged at the interface. In particular, the fluid passes forces to the solid, while the solid sends displacements back to the fluid flow. At the interface between both domains, the kinematic condition requires the velocity of the fluid (U_f) to be equal to the velocity of the solid interface (U_s). In addition, the dynamic condition ensures the compatibility of traction across the FSI interface:

$$n \cdot \sigma_s = -n \cdot \sigma_f \tag{7}$$

where n is the unit normal vector of the interface, and σ_s and σ_f denotes the solid and fluid stress, respectively. Implementing the kinematic condition, fluid nodes on the interface are updated according to their corresponding solid nodes. By doing the same for the dynamic condition, the equilibrium of stress on the fluid-solid interface is guaranteed. Then, the fluid pressure is integrated into a fluid force, which is applied to the solid nodes along with the interface.

2.4. Coupling scheme

The process flowchart for the two-way coupling algorithm is shown in Fig. 2. During a transient simulation, within one-time step, the solution for the fluid domain provides the forces acting on the structure. After interpolating the forces from the fluid mesh to the surface mesh of the structure, a solution of the structural dynamics will be attained under the effect of the acting forces.

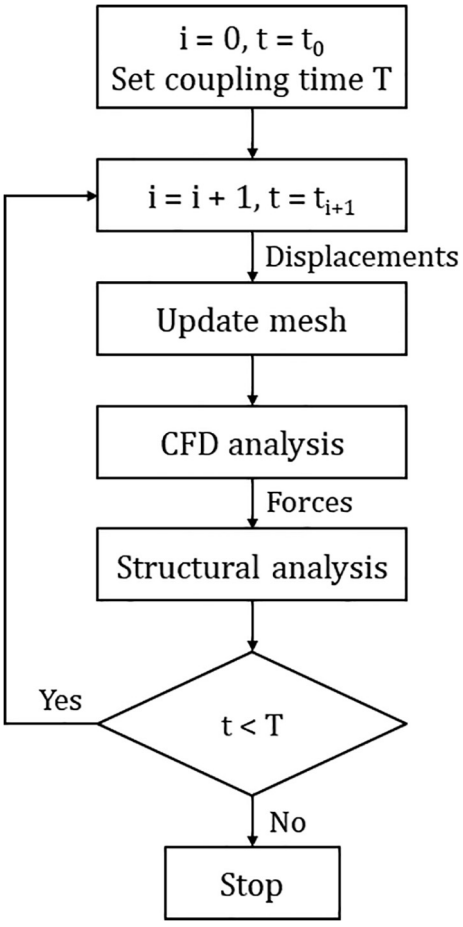

Fig. 2. Solution algorithm for two-way FSI coupling.

The response of the solid part to the emerging load represents a displacement of the structural nodes. The displacements at the boundary between solid and fluid are interpolated to the fluid mesh which leads to its deformation. This step closes one inner loop of the simulation. For strong (*implicit*) two-way coupling simulations, these steps are repeated until the changes in the flow forces and the structural displacements fall below a prescribed amount. After that, a new time step begins. The downside of this coupling technique is that the computational cost increases considerably. For weak (*explicit*) two-way FSI simulations, the convergence at the boundary between solid and fluid is not considered and a new time step is launched directly. However, at the end of the simulation, the convergence is required.

In general, an explicit scheme is easier to implement and is computationally more efficient, allowing to attain a solution similar to that obtained with an implicit scheme but in less time. In view of the available computational resources, the explicit scheme was the elected option (ANSYS Inc., 2017a).

3. Computational setup

The computational domain was built taking into account the dimensions of RMB's fuel elements. These assemblies will contain 21 plates and the dimensions are 80.5 mm × 80.5 mm × 1045 mm. The meat of each fuel plate will be made of low enriched uranium-silicide (U_3Si_2) dispersed in an aluminum matrix (Perrotta and Soares, 2015). This meat will be hermetically sealed between an aluminum alloy cladding.

A generic diagram of the studied domain is shown in Fig. 3. In the figure, the dark blue arrows indicate the fluid flow direction. In Table 1, the geometric specifications for the three cases are described. Tables 2 and 3 present the materials properties for different temperatures. In this study, in order to create an appropriate

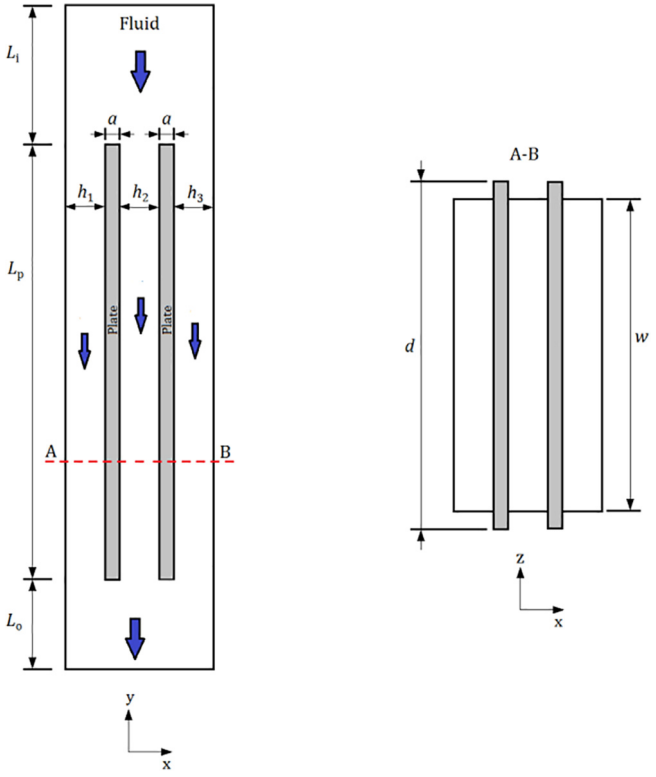

Fig. 3. Schematic diagram of the computational domain: longitudinal view (left) and top view (right). Modified from (González Mantecón and Mattar Neto, 2018).

Table 1
Geometric specifications for each case.

Parameter	Case A	Case B	Case C
Channel 1 – thickness, h_1 [mm]	2.35	2.35	2.45
Channel 2 – thickness, h_2[mm]	2.35	2.35	2.45
Channel 3 – thickness, h_3 [mm]	2.35	2.55	2.45
Fuel plates – thickness, a[mm]	1.33	1.33	1.35
Channels – width, w [mm]	70.5		
Fuel plates – width, d [mm]	75		
Inlet plenum – length, L_i [mm]	190		
Channels (fuel plates) – length, L_p[mm]	655		
Outlet plenum – length, L_o [mm]	70		

Table 2
Water properties for given temperatures.

Property	Value	
	24 °C	*50* °C
Dynamic viscosity, μ [Pa•s]	8.87×10^{-4}	5.47×10^{-4}
Density, ρ [kg/m^3]	997.6	988

Table 3
Aluminum alloy 6061-T6 properties for given temperatures.

Property	Value	
	24 °C	*120* °C
Density, ρ_m [kg/m^3]	2700	
Poisson's ratio, v	0.33	
Young's modulus, E [GPa]	68.9	64.9
Yield strength, σ_y [MPa]	276	246.5

mesh for the coupled analyses, the fluid and structural models were verified independently.

3.1. CFD model

In all three cases of interest, the fluid around the plates is water with constant physical properties (see Table 2). The fluid domain is composed of an inlet plenum, coolant channels, and an outlet plenum (see Fig. 3). It was modeled using the CFD code ANSYS CFX (ANSYS Inc., 2017a). The complete multiphysics domain is displayed in Fig. 4(a). A transparent view of this domain, near the leading edges of the plates, is presented in Fig. 4(b). It is possible to see the surfaces of the plates in contact with the fluid flow.

3.1.1. Verification of the CFD model

For all three cases, steady-state analyses with three progressively refined meshes were conducted to assess the numerical accuracy and determine the suitability of the CFD mesh for the coupled simulations. The solution verification studies were performed following the ASME CFD best-practice standard (ASME, 2009). This standard suggests the Grid Convergence Index (GCI) method to estimate and report the uncertainty due to the discretization. Generally speaking, this method is based on the selection of variables of interest or key parameters to evaluate how they vary with two or more different meshes. The aim of the method is to estimate a 95% confidence interval that contains the exact solution to the problem. For the sake of brevity, the GCI method is not described here but the formulas to calculate the GCI for the finest mesh (GCI_{12}), the refinement factor (r), the extrapolated value of the variable of interest (ϕ_{ext}^{21}) and the approximate relative error (e_a^{21}) can be found in reference (ASME, 2009). The boundary conditions for the CFD model verification analyses are given in Table 4.

The uniform inflow velocity (v_{in}) was defined by considering an inlet volumetric flow rate (Q_{in}) of 15.3 m^3/h (see Table 5). This rate of fluid flow was determined to take into account an average fluid velocity (v_0) of 8.2 m/s in the channels, which is the minimum coolant velocity required in an RMB's fuel assembly.

The fluid domain was divided into different volumes allowing the creation of hexahedral mesh. In an effort to capture the contraction/expansion effects at the leading/trailing edges of the plates, a bias factor 4:1 was set up for spacing the cells along the inlet, outlet, and channel lengths. The same bias factor was adopted for the elements along with the thickness of the channels.

The maximum pressure (P_{max}) and wall shear stress (τ_w) on the surfaces of one plate, and the pressure drop (ΔP_{cch}) through the

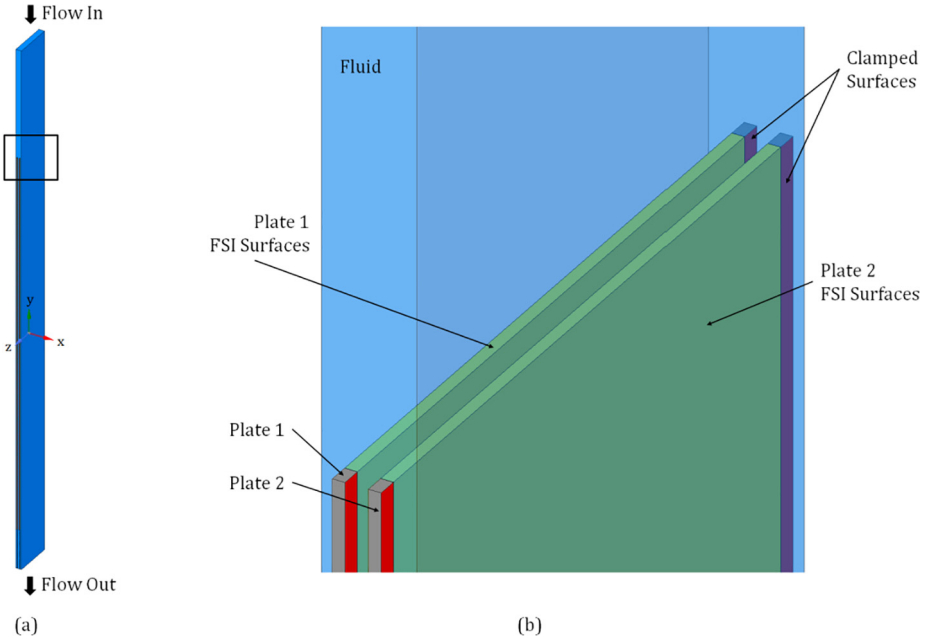

Fig. 4. Multiphysics domain. (a) Full view. (b) Transparent view close to the leading edges. The red surfaces are the regions used to clamp the fuel plates. (For interpretation of the references to colour in this figure legend, the reader is referred to the web version of this article.)

Table 4
Description of the CFD model used in the verification analyses.

Analysis type	Steady-state
Material	Water at 24 °C (properties in Table 2)
Boundary conditions	Inlet: v_{in} (see Table 5)
	Outlet: $P_{out} = 0$
	No-slip rigid walls
Turbulence model	k- ε with *scalable wall functions*
	Turbulence intensity at the inlet = 5%
Convergence criteria	RMS residuals of all conservation equation $<10^{-4}$
	Imbalances of mass and momentum <1%
	Global variables do not change with iterations

Table 5
Volumetric flow rates, velocities, and Reynolds numbers in the verification analyses.

Case	Q_{in} [m^3/h]	v_{in} [m^3/h]	Re_{in}
A	15.3	6.21	119,198
B		6.08	118,810
C		6	190,826

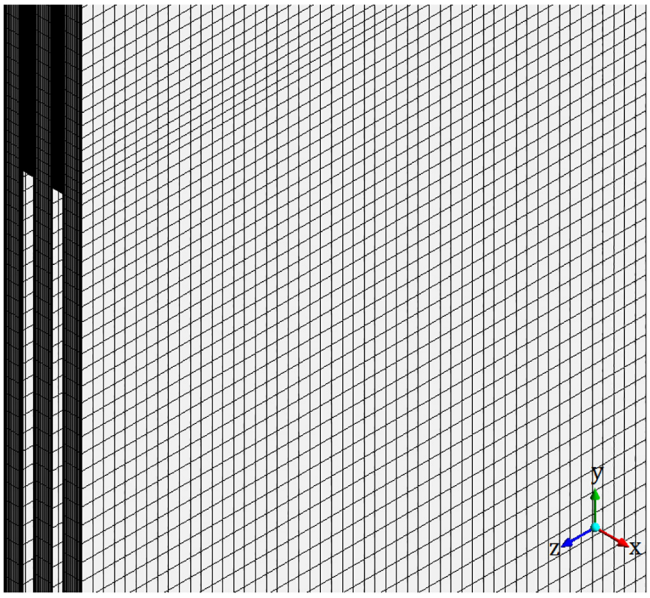

Fig. 5. Example of the mesh used in the verification of the CFD model.

central channel were selected as the key parameters. In Case B, the maximum pressure and the wall shear stress were taken from the plate located between channels with unlike thicknesses. An example of the mesh utilized in the verification of the fluid flow models is depicted in Fig. 5. Details of the three meshes for each case are summarized in Table 6, in which Mesh 1 identifies the fine mesh and Mesh 3 the coarse mesh.

Table 7
Uncertainty quantification of the CFD model.

Case	Parameter	ϕ_{ext}^{21} [Pa]	e_a^{21} [%]	GCI_{12} [%]
A	ΔP_{cch}	131,145	0.79	0.96
	P_{max}	140,648	0.24	0.09
	τ_w	198.76	0.18	0.20
B	ΔP_{cch}	122,541	0.48	0.54
	P_{max}	130,148	0.22	0.13
	τ_w	184.57	0.17	0.24
C	ΔP_{cch}	111,794	1.08	1.93
	P_{max}	113,949	0.26	0.09
	τ_w	163.43	0.23	0.31

Table 7 shows the results obtained by applying the ASME standard. It can be seen that a well-behaved convergence is obtained with all meshes. Hence, the predicted uncertainty of the key parameters can be considered as a reliable approximation of the correct solution. From the results given in tables Tables 6 and 7, we can conclude that, in each case, Mesh 1 is suitable for the fluid–solid simulations as the numerical uncertainties of the variables of interest are lower than 2%.

3.2. Structural model

The structural part of the fluid-solid domain was modeled using the FEA program ANSYS Mechanical (Transient Structural module). As mentioned before, the fuel meat of the studied plates is a fuel powder dispersed in a matrix and clad of aluminum. Thus, the considered plate material is aluminum alloy 6061-T6 (see Table 3). The plates were discretized using a structured mesh with three-dimensional solid elements SOLID186 (ANSYS Inc., 2017b). The plasticity Bilinear Isotropic Hardening model with zero Tangent Modulus is assumed.

3.2.1. Verification of the structural model

For the verification of the solid model, three different meshes were generated and static simulations were performed with ANSYS Mechanical. One plate was examined and a uniform pressure load (P) was applied over one of its long surfaces. This pressure loading is equal to the maximum pressure found in the verification of the CFD model for each case with Mesh 1. It was imposed to simulate the hydraulically induced load that the plates would be exposed to when coupled with the fluid domain. Along both sides of each plate and parallel to the fluid flow, a 2.25 mm region of the plate width was utilized to clamp them (see Fig. 3). The description of the structural model for the mesh verification studies is given in Table 8.

The plate model is depicted in Fig. 6. Twenty-two elements along the thickness of each plate were set to capture their flexural behavior with a high degree of accuracy.

Table 6
Characteristics of the meshes used in the verification of the CFD model and the values of the key parameters.

Case	Mesh	Elements	r	ΔP_{cch} (Pa)	P_{max} [Pa]	τ_w [Pa]
A	1	1,040,000	1.1435	132,156	140,550	198.44
	2	695,600	1.2462	133,196	140,206	198.08
	3	359,381	–	137,697	135,429	199.16
B	1	1,057,160	1.1173	123,073	130,014	184.21
	2	757,796	1.2723	123,668	129,725	183.90
	3	368,002	–	128,292	125,062	184.88
C	1	1,040,000	1.1436	110,097	113,869	163.03
	2	695,600	1.2462	108,908	113,574	162.66
	3	359,381	–	104,897	109,245	163.61

Table 8
Description of the structural model used in the verification analyses.

Analysis type	Static-structural
Material	Aluminum alloy 6061-T6 at 24 °C (properties in Table 3)
Boundary conditions (see Fig. 6)	Displacements x = y = z = 0 (front and back of red surfaces) Pressure (P) over a long surface of the plate.

For the uncertainty quantification due to the discretization of the structural model, the GCI method was also employed. The deflection at the midpoint (δ_M) of the plate was chosen as the main parameter for the GCI calculation. Table 9 shows the characteristic of the studied meshes and the values of the key variable. Mesh 1 is the finest mesh.

Table 10 sums up the uncertainty quantification of the structural model. It can be observed that, in all cases, the uncertainty of the finest mesh was lower than 0.5%. Therefore, in each case, Mesh 1 is chosen for the FSI calculations.

3.3. Multiphysics models

In previous subsections, the process for obtaining precise solutions of the fluid and solid domains individually is detailed. The following step was to couple these two models to investigate the behavior of the fuel plates under high-velocity flow and different geometric and materials conditions. It is important to remind that the multiphysics domain is illustrated in Fig. 4. The mesh density was established based on the aforementioned verification studies. In Table 11, some parameters of the FSI models are listed.

For the coupled models, fluid–solid interface boundary conditions were assumed on the surfaces of the plates in contact with the water. These are the surfaces where forces from the CFD analysis are applied to the structure. In the fluid domain, mesh motion of all fluid surfaces in contact with the fuel plates was allowed. In all simulations, the energy equation was neglected and double precision was adopted. For each simulation, inlet velocities of water were determined using the inlet flow rates and assumed at the inlet boundary condition. Table 12 provides those targeted values. Finally, in each case, the other conditions defined in past subsections were preserved.

Table 9
Characteristics of the meshes used in the verification of the structural model and values of the key parameters.

Case	P [Pa]	Mesh	Elements	r	δ_M [mm]
A		1	149,600	1.2488	0.5454
	140,550	2	76,800	1.2470	0.5449
		3	39,600	–	0.5439
B		1	149,600	1.2489	0.5113
	130,014	2	76,800	1.2470	0.5107
		3	39,600	–	0.5098
C		1	149,600	1.2489	0.4638
	113,869	2	76,800	1.2470	0.4633
		3	39,600	–	0.4624

Table 10
Uncertainty quantification of the structural model.

Case	Parameter	ϕ_{ext}^{21} [Pa]	e_a^{21} [%]	GCI_{12} [%]
A		0.5459	0.09	0.11
B	δ_M [mm]	0.5125	0.12	0.29
C		0.4644	0.11	0.16

In a previous study (González Mantecón and Mattar Neto, 2019), a similar approach was employed. It showed to produce reasonably accurate results, which were validated against the experimental data of Kennedy (2015).

4. Results and discussion

The first numerical analysis was carried out and the structural response of each plate was obtained. This solution was taken as an initial condition and the new simulations were conducted. Each one ran until the convergence criterion was satisfied and steady-state solutions of the flow and structure variables were achieved, e.g. fluid-dynamic force acting on the plates and pressure drop. In all simulations, the dimensionless normal distance from the wall (y^+) was checked to verify if the wall distance requirements for the k-ε model were satisfied. It was found that y^+ was between 30 and 100, which is in the proper range with the wall function approach (ANSYS Inc., 2017a).

To verify the model convergence, monitor points (A and B) were located at the midpoint of the leading edges of the fuel plates and

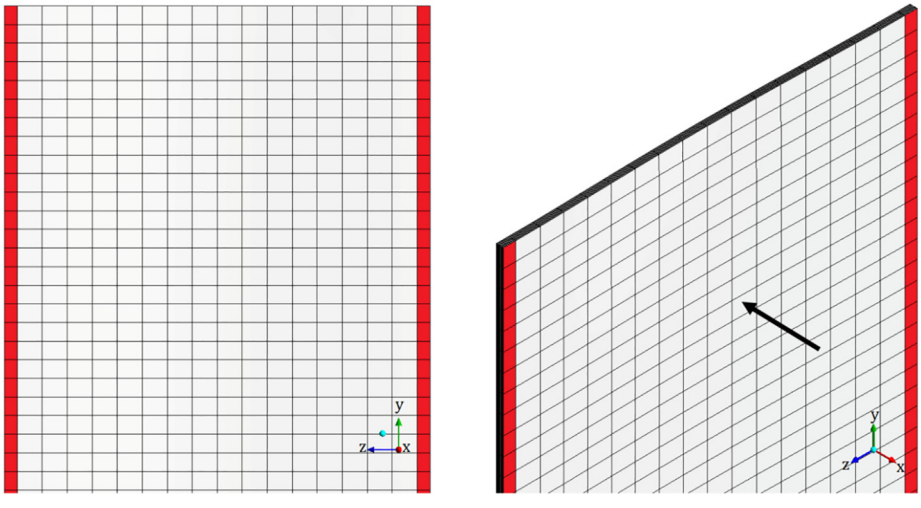

Fig. 6. Example of the mesh utilized in the verification of the solid model. The arrow indicates the direction of the application of the pressure load.

Table 11
Description of the multiphysics models.

Material	Fluid: water Solid: aluminum alloy 6061-T6
Analysis type	CFX: Transient, ANSYS Multifield Coupling Mechanical: Transient structural, large deformations enabled
Number of elements	Case A – Fluid: 1040000, Solid: 299,200 Case B – Fluid: 1057160, Solid: 299,200 Case C – Fluid: 1040000, Solid: 299,200
Boundary conditions	Fluid – Inlet: various v_{in} (see Table 12) Fluid – Outlet: $P_{out} = 0$ Fluid – No-slip moving walls (surfaces touching the plates) Fluid – No-slip rigid walls (remaining surfaces) Solid – Fluid-solid interface (surfaces bounded by the water) Solid – Displacements $x = y = z = 0$ (clamped regions)
Coupling scheme	Explicit
Time step	0.025 s
Convergence criteria	RMS residuals of all conservation equation < 10^{-4} Imbalances of mass and momentum < 1% Global variables do not change with iterations Mesh displacement residual target < 10^{-4}
Coupling data transfer	Under relaxation factor = 0.75 Convergence target = 0.01
Solution sequence	Solve ANSYS Mechanical fields before ANSYS CFX fields

Table 12
Volume flow rates and velocities used in the multiphysics simulations.

Q_{in} [m³/h]	v_{in} [m/s]		
	Case A	*Case B*	*Case C*
15.30	6.21	6.08	6.00
17.27	7.01	6.87	6.77
18.85	7.65	7.49	7.39
20.43	8.29	8.12	8.01
21.99	8.92	8.74	8.62
23.57	9.56	9.37	9.24
25.12	10.20	9.99	9.85
26.71	10.84	10.62	10.47
28.26	11.47	11.24	11.08
29.84	12.11	11.86	11.70
31.42	12.75	12.49	12.32
32.98	13.38	13.11	12.93
34.56	14.02	13.74	13.55
36.14	14.66	14.37	14.17
37.70	15.30	14.99	14.78

the total mesh displacement was extracted. Convergence history of displacement of the leading edge midpoint (Point A) of Plate 1 is here presented (see Fig. 7). This example was taken from Case C.

4.1. Results of Case A

A path was created along the axial centerline of the plates. Then, the total mesh displacement along the x-direction was extracted and plotted to give the deflection profile of each plate. Examples of these profiles are provided in Fig. 8. According to Miller (1958), and experimentally verified (Groninger and Kane, 1963; Kennedy, 2015; Smissaert, 1968), the deflection of adjacent plates are in opposite directions; this trend can be observed in the figure. Notably, the maximum deflection of each plate occurred at the leading edge, which was defined as *static divergence* (Smissaert, 1968).

In order to identify the critical velocity of the system in Case A, the relationship between the maximum deflection of the plates and the square of the average fluid velocity in the channels was considered.

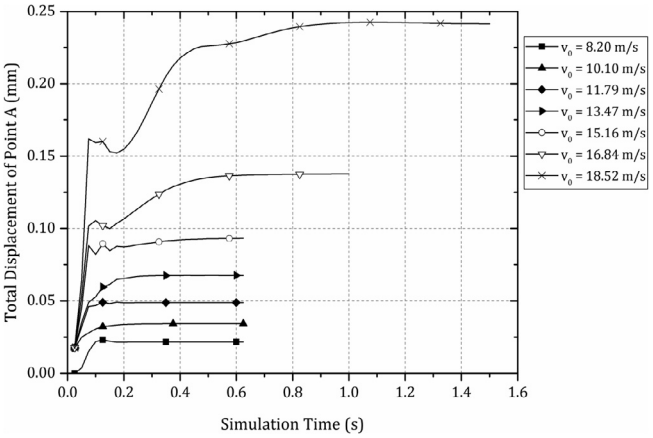

Fig. 7. Convergence history of Point A displacement for various fluid velocities in the channels.

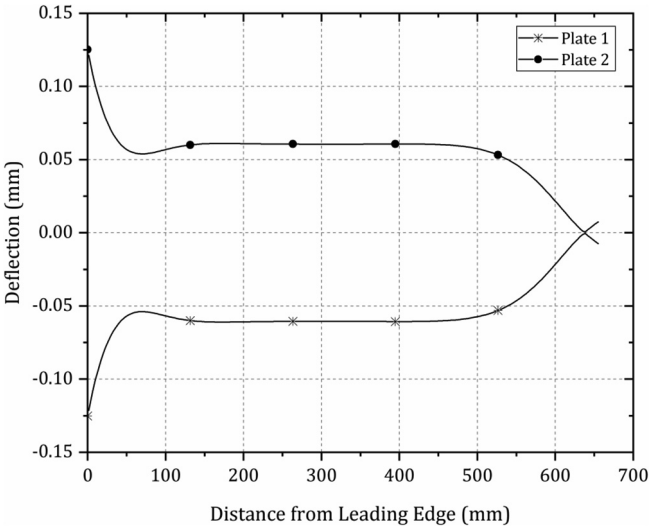

Fig. 8. Deflection profile of each plate for an inflow velocity of 12.75 m/s.

With the objective of updating current techniques applied to the design of fuel elements, a methodology was proposed in reference (González Mantecón and Mattar Neto, 2018) to predict the critical velocity by means of FSI simulations. It consists in the determination of the velocity where the maximum deflection of the plates altered from linear to nonlinear comportment with the increment of the volume flow rate. In that study, nominal dimensions of an RMB's fuel assembly and materials properties at room temperature were taken into account. Coincidentally, for these conditions, it was identified that the critical velocity determined with the numerical model was equal to Miller's velocity estimated with Eq. (1), which value is 16.84 m/s. That procedure is employed in this work.

In Fig. 9, we can note that the plotted points follow two trends. Then, two curves that fit these points were included. The first curve fit was completed up to a specific velocity and it suggests that the maximum deflection of the plates is a linear function of the squared fluid velocity in the channels. It was observed that for velocities up to that specific value, the coefficient of determination (R-Square) was higher than 0.95. On the other hand, for velocities higher than that value, it is possible to see that the maximum deflection of the plate becomes larger and it was fitted to a quadratic function. There was found that 16.68 m/s is the critical flow velocity because it is the velocity where the shape of the curve

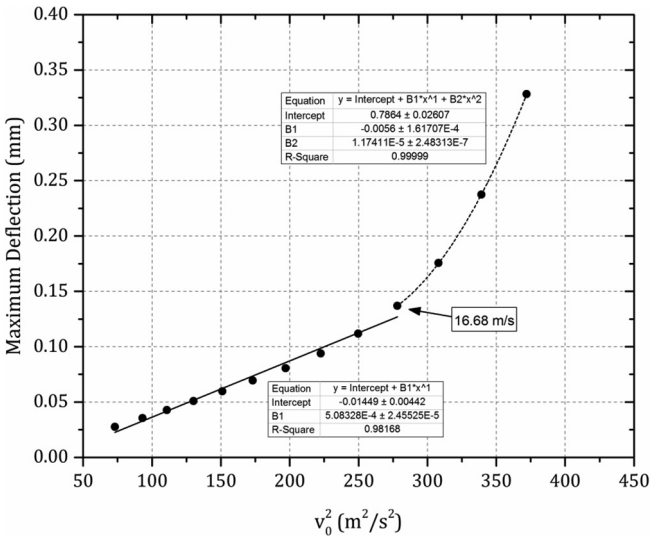

Fig. 9. Maximum deflection of Plate 1 or 2 as a function of the squared fluid velocity in the channels. The arrow indicates the critical velocity in Case A.

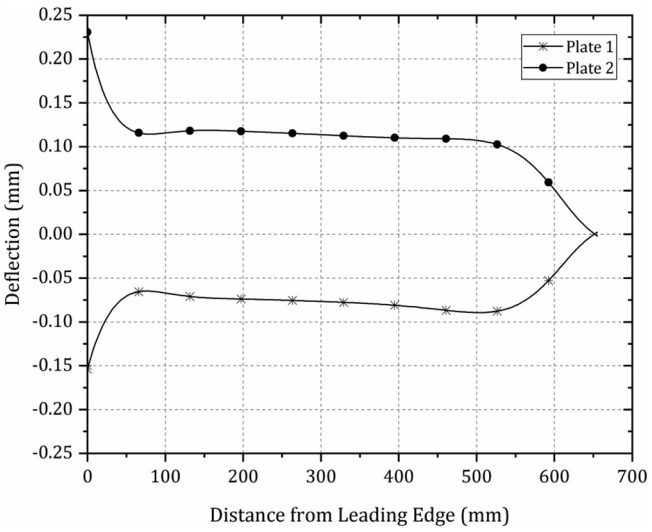

Fig. 10. Deflection profile of each plate for a fluid velocity in the channels of 17.07 m/s.

varied from linear (R-Square ≥ 0.95) to nonlinear behavior (see Fig. 9). This moment is also recognized as the beginning of the hydroelastic instability. Comparing to the result in reference (González Mantecón and Mattar Neto, 2018), the critical velocity in the current case is about 1% lower.

4.2. Results of Case B

In the second assembly, Plate 1 is located between the two-equal coolant channels and Plate 2 is flanked by the channels with different thicknesses. As can be seen in Fig. 10, the deflection of Plate 2 is larger. This is a result of a higher pressure difference between the two adjacent channels with unequal thicknesses. Furthermore, this plate deflected into the larger channel because of a bigger pressure drop in the smaller channel.

Velocity and pressure contours along the midplane of the coolant channels and near the leading edges of the plates are shown in Figs. 11 and 12, correspondingly. The flow and pressure fields in these figures demonstrate that there is a difference in pressure and flow velocity in neighboring plates. Moreover, these results show that the deflections at the leading edge of the plates play an important role in the flow redistribution between the fuel plates.

In Fig. 13, it should be noted that the total deflection of the plates is higher when different channels are considered. For this numerical experiment, the shape of the curve changes for an average fluid

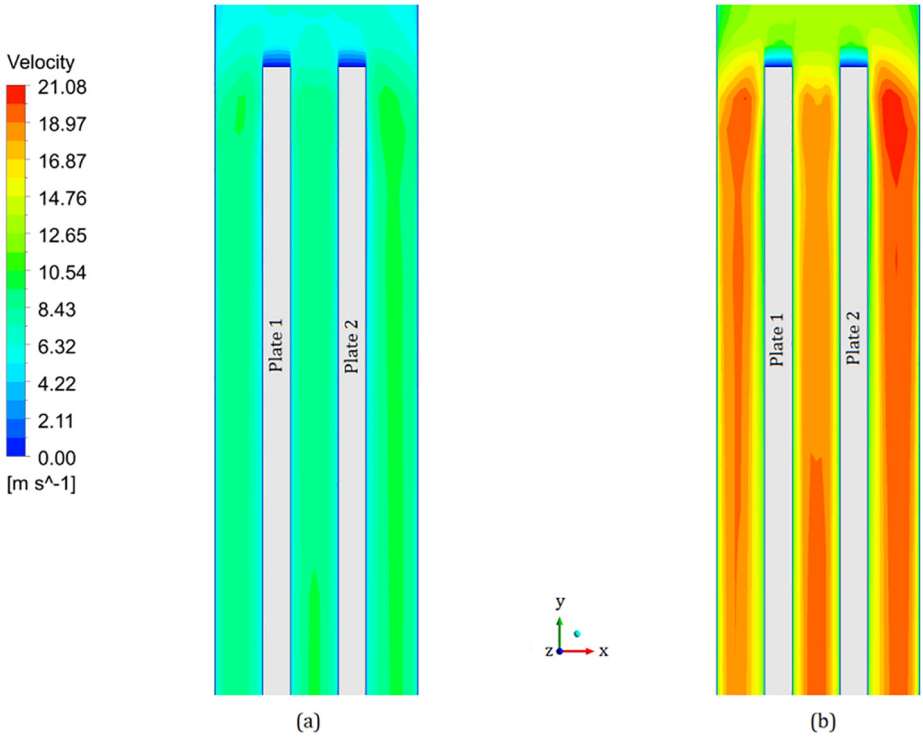

Fig. 11. Velocity contours along the midplane of the channels and near the leading edge of the plates for inflow velocities of (a) 6.08 m/s and (b) 12.49 m/s. The plates are presented undeformed and fluid flow is downward.

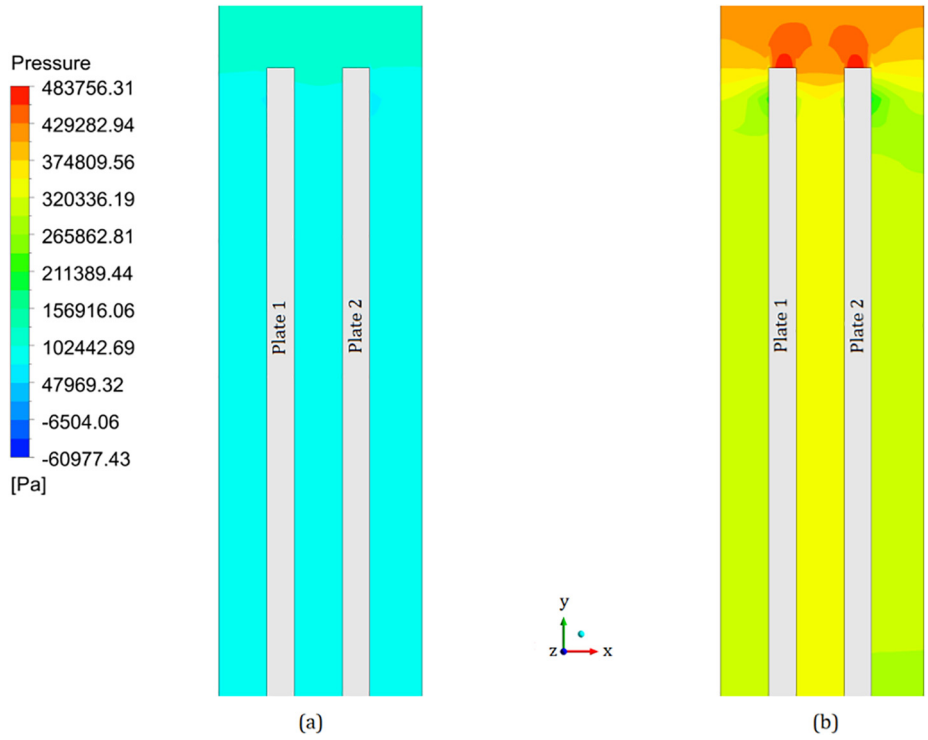

Fig. 12. Pressure contours along the midplane of the channels and near the leading edge of the plates for inflow velocities of (a) 6.08 m/s and (b) 12.49 m/s. The plates are presented undeformed and fluid flow is downward.

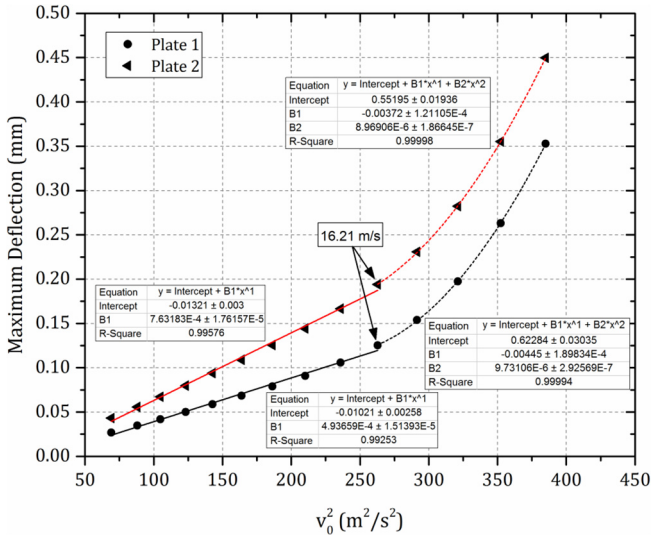

Fig. 13. Maximum deflection of each plate as a function of the squared fluid velocity in the channels. The arrows point out the critical velocity in Case B.

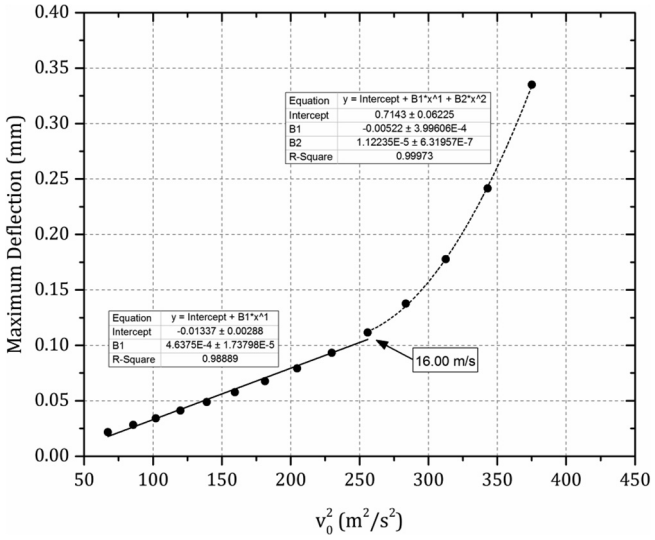

Fig. 14. Maximum deflection of Plate 1 or 2 as a function of the squared fluid velocity in the channels. The arrow indicates the critical velocity in Case C.

velocity in the channels of 16.21 m/s. This critical velocity is around 3.7% smaller than that indicated in the study with nominal dimensions. Results from this case indicate that greater deflections of the plates occur and the critical velocity may be expected at lesser velocities if initial channels deviations are present.

4.3. Results of Case C

The results from the third case are displayed in Fig. 14. For this test, the critical velocity was detected at 16 m/s. Making the comparison with the velocity determined by González Mantecón and Mattar Neto (2018), it was found that the critical flow velocity fell about 5%. This is a result of the reduction of the mechanical strength of the fuel plates with the increment of temperature.

5. Conclusions

Based on the results and by comparing to the work with nominal dimensions (González Mantecón and Mattar Neto, 2018), the following conclusions can be drawn from this study:

1) The predicted critical velocity is an indication of the flow rate at which the deflections become larger, rather than the sudden collapse of the fuel plates.
2) The results from cases A and B revealed that, if initial tolerances on fluid channel dimensions exist as a result of the fabrication process of the assemblies, deflections of the fuel plates will be amplified due to the imposed pressure difference, and the critical velocity may be expected at lower flow rates. Similarly, it was perceived that coolant channels with different thicknesses cause larger deflections than channels with smaller but equal thicknesses.
3) The influence of materials properties on flow-induced deflections of the plates was investigated in Case C. It was verified the decrease of the critical velocity magnitude with the increment of the system temperature.
4) These numerical results are qualitatively consistent with theoretical expectations and experimental investigations and have allowed gaining understandings of coupled problems in fuel elements, permitting the analysis in different conditions that would be costly to explore with experimental apparatuses.
5) In the studied cases, the plastic deformation of the plates was not detected.

The main contribution of this work is that it shows that, even if some geometric deviations from the nominal conditions due to the fabrication process are present in the fuel element, the safety factor of two-thirds of the critical velocity recommended by the IAEA could be diminished and higher flow rates could be considered. It also demonstrates the applicability of numerical simulations of fluid-structure interaction to predict the critical fluid velocity of parallel plate assemblies. Hence, representing an alternative tool that could be used during the project of new fuel assemblies.

Declaration of Competing Interest

The authors declare that they have no known competing financial interests or personal relationships that could have appeared to influence the work reported in this paper.

Acknowledgment

This work was financed by the Coordenação de Aperfeiçoamento de Pessoal de Nível Superior – Brasil (CAPES) – Finance Code 001. The authors gratefully acknowledge this support.

Appendix A. Supplementary data

Supplementary data to this article can be found online at https://doi.org/10.1016/j.anucene.2019.107118.

References

ANSYS Inc., 2017a. ANSYS CFX Documentation – Release 18.2. Canonsburg, USA.
ANSYS Inc., 2017b. ANSYS Mechanical Documentation – Release 18.2. Canonsburg, USA.
ASME, 2009. Standard for Verification and Validation in Computational Fluid Dynamics and Heat Transfer. ASME V&V 20-2009, New York, USA.
González Mantecón, J., Mattar Neto, M., 2018. Numerical methodology for fluid-structure interaction analysis of nuclear fuel plates under axial flow conditions. Nucl. Eng. Des. 333, 76–86. https://doi.org/10.1016/j.nucengdes.2018.04.009.
González Mantecón, J., Mattar Neto, M., 2019. Numerical analysis on stability of nuclear fuel plates with inlet support comb. Nucl. Eng. Des. 342, 240–248. https://doi.org/10.1016/j.nucengdes.2018.12.009.
Groninger, R.D., Kane, J.J., 1963. Flow induced deflections of parallel flat plates. Nucl. Sci. Eng. 16, 218–226. https://doi.org/10.13182/NSE63-A26503.
IAEA, 1980. Research Reactor Core Conversion from the Use of Highly Enriched Uranium to the Use of Low Enriched Uranium Fuels: Guidebook. AEA-TECDOC-233, Vienna, Austria.
Kane, J.J., 1963. The effect of inlet spacing deviations on the flow-induced deflections of flat plates. Nucl. Sci. Eng. 15, 305–308. https://doi.org/10.13182/NSE63-A26441.
Kennedy, J.C., 2015. Development and Experimental Benchmarking of Numeric Fluid Structure Interaction Models for Research Reactor Fuel Analysis Ph.D. Dissertation. University of Missouri.
Launder, B.E., Spalding, D.B., 1974. The numerical computation of turbulent flows. Comput. Meth. Appl. Mech. Eng. 3, 269–289. https://doi.org/10.1016/0045-7825(74)90029-2.
Lemoine, P., Wachs, D., 2007. High density fuel development for Research Reactors. International Conference on Research Reactors. Sydney, Australia.
Miller, D.R., 1958. In: Critical Flow Velocities for Collapse of Reactor Parallel-Plate Fuel Assemblies. Report No. KAPL-1954. Knolls Atomic Power Laboratory Schenectady, USA. https://doi.org/10.2172/4199355.
Perrotta, J.A., Soares, A.J., 2015. RMB: the new Brazilian multipurpose research reactor. Int. J. Nucl. Power 60, 30–34.
Smissaert, G.E., 1968. Static and dynamic hydroelastic instabilities in MTR-type fuel elements Part I. Introduction and experimental investigation. Nucl. Eng. Des. 7, 535–546. https://doi.org/10.1016/0029-5493(68)90103-9.